N.A.E.

R. & M. 2727
(13,034)
A.R.C. Technical Report

MINISTRY OF SUPPLY

Royal Aircraft Establishment
25 MAR 1954
LIBRARY

AERONAUTICAL RESEARCH COUNCIL
REPORTS AND MEMORANDA

A New Relaxational Treatment of the Compressible Two-dimensional Flow about an Aerofoil with Circulation

By

L. C. Woods, D.Phil. and A. Thom, M.A.,
Engineering Department, The University, Oxford

Crown Copyright Reserved

LONDON: HER MAJESTY'S STATIONERY OFFICE
1953

FIVE SHILLINGS NET

A New Relaxational Treatment of the Compressible Two-Dimensional Flow about an Aerofoil with Circulation

By

L. C. Woods, D.Phil., and A. Thom, M.A.,
Engineering Department, The University, Oxford

*Reports and Memoranda No. 2727**
March, 1950

Royal Aircraft Establishment
25 MAR 1954
LIBRARY

Summary.—The incompressible two-dimensional flow about an aerofoil with circulation is calculated using relaxation on the square mesh formed by the incompressible velocity equipotentials (ϕ = constant) and the streamlines (ψ = constant). Log $(1/q_0)$ and θ_0, where (q_0, θ_0) is the incompressible velocity vector on polar co-ordinates, are harmonic functions in the (ϕ, ψ)-plane, and can be found by well-known relaxation or squaring methods. Boundary conditions are specified in the (x, y) or physical plane, but starting from an assumption for the surface velocity, approximate boundary conditions can be found for the (ϕ, ψ)-plane, which then enable a more accurate value of the surface velocity to be calculated, and so on. The circulation is imposed on the field by having a smaller number of equipotential lines of the mesh cutting the lower surface of the aerofoil than cutting the upper surface.

Non-linear compressible flow equations involving log $(1/q)$ and θ, where (q, θ) is the compressible flow vector, are solved by relaxation on the (ϕ, ψ) grid. The results for a worked example are compared with experimental curves provided by the National Physical Laboratory for the same aerofoil at approximately the same angle of incidence. There is reasonable agreement. Supersonic patches were experienced and are not difficult to treat by relaxation, although the difference equations become poorly conditioned.

Nomenclature

(x, y)	Physical plane, in which $z = x + iy$
(ϕ, ψ)	The transformed incompressible flow plane in which the aerofoil is represented by a slit on $\psi = 0$. $w = \phi + i\psi$
(q_0, θ_0)	Incompressible velocity vector in polar co-ordinates. θ_0 is the angle between the x-axis and the velocity vector
L_0	$= \log (1/q_0)$
q, L, θ	Similar quantities for compressible flow
α	Angle between the compressible and incompressible velocity vectors
δ	$= L - L_0$
β	Angle of incidence measured from the chord
c	Aerofoil chord length
β_0	Zero-lift angle
R	Radius of curvature of the boundary
n	Interval of the square mesh

* Oxford University Engineering Laboratory Report No. 35.

A

Nomenclature—continued

s	Distance along a boundary or streamline
X	Residual of the relaxation process
V	Undisturbed stream velocity, taken throughout as unity
M	Local Mach number
M_0	Undisturbed stream Mach number
q_s	Incompressible velocity on the aerofoil surface
a	Local velocity of sound
a_0	Stagnation sound velocity
∇^2	$\partial^2/\partial\psi^2 + \partial^2/\partial\phi^2$
A	Front stagnation point
H	Rear stagnation point

---

1. *Introduction.*—It was decided that the most suitable shape of aerofoil for investigation would be one for which full experimental results were available at a range of Mach numbers. An aerofoil that had shown unusual freedom from shock-waves in the National Physical Laboratory High Speed Tunnel was selected as a suitable example. The aerofoil was NACA 16, a 10 per cent propeller aerofoil designed for high speed. Table 1 gives the profile co-ordinates provided by the National Physical Laboratory. They also provided experimental results for comparison with the theoretical solution, and since these were given for an angle of incidence of 1·4 deg, it was decided to aim as close as possible to this angle. All calculations were carried out in the (ϕ, ψ)-plane in which the aerofoil is represented by a slit along $\psi = 0$. The ends of the slit represent the stagnation points for incompressible flow. For zero circulation there must be as many equipotentials of the square mesh cutting the upper edge of the slit as cutting the lower edge. The circulation can be secured about an aerofoil by arranging that there are a different integer number of equipotential lines of the mesh cutting each edge of the slit representing the aerofoil surface. This method was adopted and Fig. 1b shows the type of field in which the relaxation was carried out. Log $(1/q)$ $(= L)$ was the dependent variable of the relaxation. For incompressible flow L_0, and θ_0 are conjugate harmonic functions, R. & M. 2726 gives the details of the relaxation solution of

$$\nabla^2 L_0 = 0 \qquad \ldots \qquad (1)$$

subject to the boundary conditions

$$\frac{\partial L_0}{\partial \psi} = \frac{1}{Rq_s} \qquad \ldots \qquad (2)$$

on the aerofoil surface. L_0 becomes infinite at stagnation points and sharp corners, and a special treatment is necessary at these singularities (R. & M. 2726).

For compressible flow it can be shown that (R. & M. 2731[3])

$$\nabla^2 L \simeq \frac{\partial}{\partial\phi}\left(M^2\frac{\partial L}{\partial\phi}\right) + \frac{\partial}{\partial\phi}\left(M^2\alpha\frac{\partial L}{\partial\psi}\right) + \frac{\partial}{\partial\psi}\left(M^2\alpha\frac{\partial L}{\partial\phi}\right) \qquad \ldots \qquad (3)$$

which assumes that α, the angle between the compressible and incompressible-flow vectors, is small enough for its squares and higher powers to be neglected. The boundary conditions are

$$\frac{\partial L}{\partial \psi} = \frac{\partial L_0}{\partial \psi} = \frac{1}{Rq_s} \cdot \qquad \ldots \qquad (4)$$

The terms involving α in (3) can be ignored with little loss in accuracy, and so

$$\nabla^2 L = \frac{\partial}{\partial \phi}\left(M^2 \frac{\partial L}{\partial \phi}\right). \qquad \ldots \qquad (5)$$

α cannot be ignored at the front stagnation point since it indicates the movement of this stagnation point off the incompressible flow grid. A relaxation treatment of (5) has been given (R. & M. 2731[3]). Fig. 2 shows the relaxation pattern employed, for the diamond labelled 1, 2, 3, 4 in Fig. 1b. If α is required it can be calculated from

$$\nabla^2 \alpha \doteq -\frac{\partial}{\partial \psi}\left(M^2 \frac{\partial L}{\partial \phi}\right), \qquad \ldots \qquad (6)$$

which can be applied when L has been approximately calculated using (5). When (6) has been solved it becomes possible to allow for the terms involving α in (3). Alternatively the equations (R. & M. 2731[3])

$$\frac{\partial \alpha}{\partial \psi} - \frac{\partial \delta}{\partial \phi} = -M^2\left(\frac{\partial L}{\partial \phi} + \alpha \frac{\partial L}{\partial \psi}\right), \quad \frac{\partial \alpha}{\partial \phi} + \frac{\partial \delta}{\partial \psi} = M^2 \alpha \frac{\partial L}{\partial \phi} \qquad \ldots \qquad (7)$$

can be used to compute α from the known L-field. Suitable difference equations representing (7), for the mesh labelled in Fig. 1, are

$$\alpha_3 \doteq \alpha_1 + (M^2\alpha)_5 (L_3 - L_1) - (\delta_2 - \delta_4)$$

$$\alpha_2 \doteq \alpha_4 + (\delta_1 - \delta_3) - M_5^2(L_1 - L_3) - (M^2\alpha)_5 (L_2 - L_4). \qquad \ldots \qquad (8)$$

It had been found that for a circular cylinder in a compressible fluid with a Mach number high enough for supersonic patches to appear ($M_0 = 0{\cdot}425$), α was never greater than 3 deg, and so in the aerofoil example of this paper α was ignored, except at the front stagnation point (A). Equations (7) enabled an integration to be carried out from the aerofoil surface, where $\alpha = 0$, into the field and then to the front stagnation streamline, then along this stream line to the mesh point adjacent to A. Extrapolation then enabled α at A, and hence the actual movement of the stagnation point off the incompressible grid, to be determined.

The aerofoil was taken to be situated in an open stream and so the boundary condition at infinity was $L = 0$ (since the undisturbed stream velocity is taken to be unity). However an outer boundary condition at between two to three chords radius from the aerofoil centre was calculated theoretically, by replacing the aerofoil by a substitution vortex[5]. The only alternative to this is the inversion of the w-plane to limit the field, but this is not a very convenient procedure with numerical methods, and further the existence of circulation and compressibility make it quite impractical.

A. *Incompressible Flow.*

The suffix $_0$ to denote incompressible values will be generally omitted in this section, since only incompressible quantities appear.

1. *Glauert's Thin Aerofoil Theory.*—While the method of computing incompressible flow given in R. & M. 2726, and outlined below in section 4, is independent of the accuracy of an initial guess for $q_s = q_s(\phi)$, nevertheless it saves labour if this initial guess is relatively accurate. To this end Glauert's thin-aerofoil theory has been used to determine an approximate solution as a starting point.

The values of $q(x/s)$ calculated from Glauert's theory are shown graphed in Fig. 4. These are for an angle of incidence $\beta = 1{\cdot}54$ deg. The theory also yields $\beta_0 = 2{\cdot}28$ deg which compares favourably with the experimental result of $2{\cdot}3$ deg, although this agreement is a little fortuitous, as indicated in section 6.

2. *The Substitution Vortex.*—The x-axis is taken to be along the chord in this and following sections. A vortex of strength K at the origin of the z-plane, in a uniform stream of unit velocity at an angle of incidence β, gives rise to a w-plane (or stream function) defined by

$$w = ze^{i\beta} + \frac{iK}{2\pi} \log z \quad .. \quad .. \quad .. \quad .. \quad .. \quad .. \quad .. \quad (9)$$

i.e.,

$$\phi + i\psi \simeq x - \frac{K\gamma}{2\pi} + i\left(y + \frac{K}{2\pi} \log r\right) \quad .. \quad .. \quad .. \quad .. \quad (10)$$

where $z = re^{i\gamma}$, and β is neglected with negligible error. Since $\gamma \simeq \tan^{-1}(\psi/\phi)$, and $r \simeq (\phi^2 + \psi^2)^{1/2}$ at large values of r, from (10) we have approximately

$$x = \phi + \frac{K}{2\pi} \tan^{-1}(\psi/\phi),\ y = \psi - \frac{K}{2\pi} \log \sqrt{(\phi^2 + \psi^2)} \quad .. \quad .. \quad .. \quad (11)$$

from which can be calculated $r = \sqrt{(x^2 + y^2)}$, $\gamma = \tan^{-1}(y/x)$ for any given (ϕ, ψ).

Also from (9)

$$qe^{-i\theta} \frac{dw}{dz} \equiv \cos\beta + \frac{K}{2\pi r} \sin\gamma + i\left(\sin\beta + \frac{K}{2\pi r} \cos\gamma\right)$$

i.e.,

$$q^2 = 1 + \frac{K}{\pi r} \sin(\gamma + \beta) + \left(\frac{K}{2\pi r}\right)^2,\ \theta = \tan^{-1} \frac{\sin\beta + (K/2\pi r)\cos\gamma}{\cos\beta + (K/2\pi r)\sin\gamma}$$

or since $r >> K$ and β is small,

$$L \equiv \log \frac{1}{q} \simeq -\frac{K}{2\pi r} \sin\gamma, \text{ and } \theta = \beta + \theta_1, \text{ where } \theta_1 = \frac{K}{2\pi r} \cos\gamma. \quad .. \quad (12)$$

Thus, given K, (11) and (12) enable $L_c = L(\phi_c, \psi_c)$ and $\theta_c = \theta(\theta_c, \psi_c)$ to be found on the outer boundary (ϕ_c, ψ_c).

The substitution vortex should be placed at the centroid of circulation (x_e, y_e) where

$$x_e = \frac{1}{K} \int xq\, ds,\ y_e = \frac{1}{K} \int yq\, ds, \quad .. \quad .. \quad .. \quad .. \quad .. \quad .. \quad (13)$$

which cannot be calculated until the solution is known. However using the results from Glauert's theory (x_e, y_e) can be calculated approximately, which is sufficient, since the values of L and θ at distances of two to three chords radius are little affected by relatively large variations in the position of the substitution vortex. In fact the centroid of circulation could be taken at the quarter-chord point with little loss in accuracy[5].

The accuracy of the substitution vortex was investigated by calculating values of L by the method of this section at a radius of about one-and-a-half chords from the aerofoil centre and comparing them with the relaxation results obtained in a field the outer boundary of which was at about two-and-a-half chords radius. The maximum deviation of the substitution vortex values of (12) from the relaxation values was 1 per cent while the standard deviation was 0·4 per cent. The greatest errors were on the portions of the boundary immediately in front and behind the aerofoil. The standard deviation on the two thirds of the boundary which excluded these portions was only 0·1 per cent. At two-and-a-half chords radius these errors would be much smaller.

3.1. *The Circulation.*—The following approximate theory is of assistance when deciding on the arrangement of the mesh about the aerofoil.

From aerofoil theory $K = \frac{1}{2}cC_L$, and from Glauert's thin-aerofoil theory $C_L = 2\pi(\beta + \beta_0)$, and so approximately,

$$K = \pi c(\beta + \beta_0). \qquad (14)$$

The origin for x, s, and ϕ will be taken at H, the trailing edge. The value of ϕ at A, the front stagnation point, will depend upon the path taken from H to A. Suppose ϕ_U and ϕ_L are the values of ϕ at A obtained by taking paths along the upper and lower surfaces respectively, then the potential jump at A, $\phi_U - \phi_L$, is equal to the circulation K. c can be written approximately $\frac{1}{2}(\phi_U + \phi_L)$, and (14) becomes

$$\frac{\phi_U - \phi_L}{\phi_U + \phi_L} = \frac{\pi}{2}(\beta + \beta_0), \qquad (15)$$

in which β is known and β_0 can be taken from Glauert's theory. The values of ϕ_U and ϕ_L must be selected so that (15) is approximately satisfied, and are such that the stagnation points fall on the mesh. Thus the closeness with which (15) can be satisfied depends upon the amount of subdivision of the mesh near the nose.

Results at a specified angle of incidence could be obtained by the interpolation of results found at several angles of incidence by varying the circulation a discrete amount each time.

3.2. *The Angle of Incidence.*—The actual angle of incidence for a given value of ϕ_U and ϕ_L remains to be found. Suppose that by relaxation a solution $L = L(\phi, \psi)$ has been found. Integration of the Cauchy-Riemann equations connecting L and ϕ yields

$$\theta(\phi, \psi) = \theta(\bar{\phi}, \bar{\psi}) + \int_{\bar{\psi}}^{\psi} \frac{\partial L}{\partial \phi}\, d\psi - \int_{\bar{\phi}}^{\phi} \frac{\partial L}{\partial \psi}\, d\phi. \qquad (16)$$

$\theta(\bar{\phi}, 0)$ on the aerofoil is known, and so integrating to the outer boundary at (ϕ_c, ψ_c)

$$\theta_c = \theta_c(\phi_c, \psi_c) = \theta(\bar{\phi}, 0) + \int_{0}^{\psi_c} \frac{\partial L}{\partial \phi}\, d\psi - \int_{\bar{\phi}}^{\phi_c} \frac{\partial L}{\partial \psi}\, d\phi. \qquad (17)$$

From (12)

$$\theta_c(\phi_c, \psi_c) = \beta + \theta_1(\phi_c, \psi_c), \text{ i.e., } \beta = \theta_c - \theta_1 \qquad (18)$$

in which θ_c is calculated from (17), and θ_1 from (12). Since the substitution vortex is an approximation only, β, calculated from (18), can be expected to be a function of (ϕ_c, ψ_c) instead of a constant. However the average value of β so found will be reasonably accurate.

4. *Outline of the Method.*—Following is a summary of the steps to be taken to find by relaxation the incompressible flow about an aerofoil with circulation. In practice, of course all the differentiations and integrations of this section are performed numerically.

(i) Determine from the profile co-ordinates

(a) $$\frac{s}{c} = \frac{s}{c}\left(\frac{x}{c}\right) = \int_0^{x/c} \left[1 + \left(\frac{dy}{dx}\right)^2\right]^{1/2} d\left(\frac{x}{c}\right), \qquad (19)$$

(b) semi-perimeter $p = mc$ say, from

$$p = \tfrac{1}{2}\oint \left[1 + \left(\frac{dy}{dx}\right)^2\right]^{1/2} d\left(\frac{x}{c}\right), \qquad (20)$$

in which $\oint$ denotes integration right round the profile ;

$$\text{(c)} \quad \frac{c}{R} = \frac{c}{R}\left(\frac{x}{c}\right) = c\,\frac{d^2y}{dx^2}\left[1+\left(\frac{dy}{dx}\right)^2\right]^{-1\frac{1}{2}} \quad \ldots\ldots\ldots\ldots\ldots \quad (21)$$

(ii) Find ϕ_U and ϕ_L from (15), and set out the mesh in the (ϕ, ψ)-plane.

(iii) Use (12), in which $K = \phi_U - \phi_L$, to determine L and θ on an outer boundary at two to three chords radius.

(iv) Assume or calculate from Glauert's thin-aerofoil theory an approximate

$$q_s = q_s(\phi). \quad \ldots\ldots\ldots\ldots\ldots\ldots\ldots \quad (22)$$

($q_s = 1$ *could* be taken as the initial assumption).

(v) Since

$$s(\phi) = \int_0^{\phi} \frac{d\phi}{q_s(\phi)}, \text{ and from (20) } c = \frac{1}{2m}\int \frac{d\phi}{q_s(\phi)}, \quad \ldots\ldots \quad (23)$$

then $\frac{s}{c}(\phi) = 2m \int_0^{\phi} \frac{d\phi}{q_s(\phi)} \Big/ \left(\int \frac{d\phi}{q_s(\phi)}\right)$, hence from (19) and (21) we can find $\frac{c}{R} = \frac{c}{R}(\phi)$. (24)

The boundary condition, $\frac{\partial L}{\partial \psi} = \frac{1}{c}\frac{c}{R}\frac{1}{q_s}$, $\ldots\ldots\ldots\ldots\ldots\ldots$ (25)

follows from (22), (23) and (24).

(vi) Laplace's equation subject to the boundary condition (25), is now solved by relaxation in the (ϕ, ψ)-plane. The singularities ($L = \infty$) at A and H are treated by the methods of R. & M. 2726. From this solution a more accurate $q_s = q_s(\phi)$ is obtained to use in step (iv).

(vii) Steps (v) and (vi) are repeated until q_s remains unchanged.

(viii) Equation (13) is used to find the position of the centroid of circulation, and if this is far from the quarter-chord point the outer boundary values will alter slightly, necessitating further relaxation.

When this is complete we will have

$$L = L(\phi, \psi), \quad \ldots\ldots\ldots\ldots\ldots\ldots \quad (26)$$

and using (16) we can find

$$\theta = \theta(\phi, \psi).$$

(ix) The (ϕ, ψ) and (x, y)-planes are now related by

$$\left.\begin{aligned} x = x(\phi, \psi) &= \int_{\bar{\phi}}^{\phi} \frac{\cos\theta}{q}\,d\phi - \int_{\bar{\psi}}^{\psi} \frac{\sin\theta}{q}\,d\psi, \\ y = y(\phi, \psi) &= \int_{\bar{\phi}}^{\phi} \frac{\sin\theta}{q}\,d\phi + \int_{\bar{\psi}}^{\psi} \frac{\cos\theta}{q}\,d\psi, \end{aligned}\right\} \quad \ldots\ldots \quad (27)$$

and hence from (26) we have $L_0 = L_0(x, y)$, $\theta_0 = \theta_0(x, y)$.

(x) Finally the angle of incidence is found from (18).

Instead of relaxing to find $L_0(\phi, \psi)$, and then integrating to find $\theta_0(\phi, \psi)$, we could have relaxed to find θ_0, which had fixed boundary values, and then integrated to find L_0. Generally, however, the prime aim of an investigation is to find q_s, and for this it is more direct to relax the L-field. Also numerical integration is likely to involve cumulative errors which can be largely avoided in relaxation by arranging that the small unrelaxed residuals sum to zero over blocks of squares.

5. *An Example: NACA* 16.—This aerofoil, and the reasons for selecting it as an example received some attention in the introduction. Glauert's thin-aerofoil theory gave $\beta_0 = 2{\cdot}3$ deg, and since the experimental results were for $\beta = 1{\cdot}4$ deg, these values were used in (15) to enable a suitable (ϕ, ψ)-mesh to be selected. The mesh selected was such that along the main portion of the aerofoil the mesh size was one unit of velocity potential. At the nose the mesh was graded down to 1/128th of a unit, while at the outer boundary the mesh size was 8 units. In all over eight hundred mesh points were involved, *i.e.*, eight hundred simultaneous equations had to be solved.

In R. & M. 2726 the treatment of the singularities at the stagnation points is based on the approximate equation

$$L_0(\phi, \psi) = \frac{\tau}{2\pi} \log \sqrt{(\phi^2 + \psi^2)} \qquad (28)$$

in which τ is the leading or trailing edge angle and the origin is at the singularity. Equation (28) is a valid approximation only if $\sqrt{(\phi^2 + \psi^2)}$ is small relative to R near the stagnation point. This condition is easy to satisfy at sharp trailing edges since R is generally large in their vicinity but at the nose of a small nose radius aerofoil the condition is satisfied at mesh points neighbouring the stagnation point, only if the mesh is very fine. This was the reason for the very fine mesh used in the example.

Now on the profile

$$\int d\theta + \tau_A + \tau_H = 0,$$

is simply one of the conditions that the profile is closed. With a finite number of mesh points on the boundary, say m of them, then the condition becomes

$$\sum_{i=1}^{m} \delta\theta_i + \tau_A + \tau_H = 0, \text{ or}$$

since $$\delta\theta = -\frac{\partial L}{\partial \psi}\delta\phi = -\frac{\delta\phi}{Rq_s}, \text{ then } \tau_A = -\sum_{i=1}^{m}\left(\frac{\delta\phi}{Rq_s}\right)_i - \tau_H. \qquad (29)$$

In order to secure closure of the profile, equation (29) must be satisfied exactly regardless of the real value of τ_A. As $m \to \infty$, $\tau_A \to \pi$, but even with the very small mesh near the nose in the present example (29) gave $\tau_A = 135$ deg instead of 180 deg.

The exact location of the front stagnation point A was very important since it was found that a movement of A a distance of $c/1{,}000$ along the profile altered the velocity peak, which occurred at $0{\cdot}01c$, by as much as 10 per cent. Integration from the trailing edge is likely to involve cumulative errors and so an alternating method of locating A was used. This was to use (16) to find θ at A (θ_A), by integrating through the field from some point on the aerofoil boundary, where θ is known, to the stagnation streamline, then along this streamline to A. Extrapolation was used over the last mesh interval. Knowing that the boundary at A was at an angle of $\theta_A + \pi/2$ to the chord, it was a simple matter with a large scale drawing of the nose and a protractor to find the position of A. This process was carried out several times during the relaxation. The final value of θ_A was 27 deg ; from which it was deduced that A was at $x/c = 0{\cdot}0025$ on the under surface.

No other special difficulties arose.

6. *Discussion of Results.*—In Fig. 6 the flow pattern and equivelocity contours are shown. The lines of equal values of θ are a family of curves orthogonal to the equivelocity curves. Table 2 sets out the pressure coefficients. In Fig. 4 the pressure distribution is compared with pressures calculated for $M_0 = 0$ from the experimental results at $M_0 = 0{\cdot}4$ by Glauert's correction,

i.e., $$C_{p,(M_0=0)} = (1 - M_0^2)^{1/2}\, C_{p,(M_0=0{\cdot}4)}.$$

This procedure was adopted since experimental results at lower speeds were not available. Also plotted in this figure are the results obtained from Glauert's thin-aerofoil theory.

The experimental results indicate a loss of lift from that theoretically possible, which loss is due to the divergence of the experimental and theoretical pressure curves towards the trailing edge. This can be explained as due to the increase in thickness of the boundary layer as the trailing edge is approached. Agreement between the curves is good in the range $0 \leqslant x/c \leqslant 0{\cdot}6$. The curve obtained from Glauert's theory is not very accurate although it has nearly the same general shape as the relaxation curve. In fact if β_0 is increased from $2{\cdot}3$ deg to $2{\cdot}7$ deg Glauert's theory reproduces the relaxation results very closely.

One disadvantage of the relaxation method is that it offers no method of calculating β_0 apart from completely recalculating the problem at zero circulation. By an application of (18) β was found to be $1{\cdot}54$ deg. The value of C_L found from the relaxation curve of Fig. 4 was $0{\cdot}510$, also from $C_L = 2K/c$ we find the same value of $C_L = (0{\cdot}510)$. A further method of calculating C_L is as follows. If $4r$ is the length of the slit in the (ϕ, ψ)-plane representing the aerofoil at zero incidence (*i.e.*, r is the radius of the circle which transforms into the aerofoil), then we have exactly[5]

$$C_L = 2\pi(\beta + \beta_0) \,.\, 4r/c. \qquad \ldots \quad \ldots \quad \ldots \quad \ldots \quad \ldots \quad \ldots \quad \ldots \qquad (30)$$

For a first approximation $4r = c$, and substituting $\beta = 1{\cdot}54$ deg (relaxation result) and $\beta_0 = 2{\cdot}3$ deg (experiment and Glauert), in (30) yields

$$C_L = 2\pi(1{\cdot}54 + 2{\cdot}3) \,.\, \pi/180 = 0{\cdot}421,$$

and unless $c/4r = 421/510 = 0{\cdot}825$, which is most unlikely for a thin aerofoil, this value of C_L is too small. At this stage it seemed that the error was most likely to be in the value of β_0. The boundary layer would have an effect on the experimental value of β_0, and Glauert's theory is only approximate. This view was confirmed some time later by an entirely new approach termed the ' polygon method '[8]. This new method of calculating the incompressible flow about an arbitrarily shaped aerofoil is based on the solution of an integral equation and is much quicker than relaxation.

From the polygon method it was found that $c/4r = 0{\cdot}9268$ and $\beta_0 = 2{\cdot}27$ deg. Thus with $\beta = 1{\cdot}54$ deg and $\beta_0 = 2{\cdot}73$ deg equation (30) gives $C_L = 0{\cdot}505$, which agrees closely with the relaxation result. Further from the polygon method it was found that at an absolute angle of incidence of $\beta + \beta_0 = 1{\cdot}54$ deg $+ 2{\cdot}72$ deg $= 4{\cdot}26$ deg, A was at $x/c = 0{\cdot}0026$ from the leading edge, which compares very well with the relaxation result which was $0{\cdot}0025$. Also it has been remarked above that the results from Glauert's theory agree closely with the other results if β_0 is increased from $2{\cdot}3$ deg to about $2{\cdot}7$ deg. All these points seem to indicate that, theoretically at least, β_0 should not be taken as $2{\cdot}3$ deg, but as $2{\cdot}72$ deg. It seems that in this case the effect of the boundary layer is to reduce β_0. The experimental value of C_L (by extrapolation to $M_0 = 0$, *see* Fig. 10) is $C_L = 0{\cdot}43$, which is about 16 per cent less than the theoretical value. This corresponds in (30) to a reduction of β_0 by $0{\cdot}7$ deg ; but of course as the incidence changes the boundary layer will change and the loss in lift will be less at the smaller angles of incidence. Thus it would seem that the boundary layer has resulted in a reduction of β_0 by $0{\cdot}4$ deg.

B. *Compressible Flow.*

Incompressible values are distinguished in this section by the suffix $_0$.

7. *The Relaxation Solution.*—The mesh is the same as that used for incompressible flow, and so it is only necessary to find $L = L(\phi, \psi)$ then from (27) $L = L(x, y)$ follows immediately.

Equation (5) is solved by relaxation (R. & M. 2731[3]) subject to the same aerofoil boundary conditions as for incompressible flow (*see* (4)). The outer boundary conditions calculated from the substitution vortex require modifying as follows.

Glauert's correction[5], relates the incompressible circulation K_0 to the compressible circulation K by

$$K = K_0\sqrt{(1 - M_0^2)},$$

and so (12) becomes

$$L \simeq \frac{K_0 \sin\gamma}{2\pi r\sqrt{(1-M_0^2)}}, \quad \theta = \beta + \frac{K_0 \cos\gamma}{2\pi r\sqrt{(1 - M_0^2)}}. \qquad (31)$$

In R. & M. 2731[3] it is shown that the residuals X for equation (5) are best calculated from (*see* Fig. 1) :—

$$X_5 = (1 - M_5^2)L_1 + L_2 + (1 - M_5^2)L_3 + L_4 - 2(2 - M_5^2)L_5 + \tfrac{1}{2}M_5^2\left(\frac{a_0}{a}\right)^2(L_1 - L_3)^2, \qquad (32)$$

but that the most convenient relaxation pattern is (Fig. 2)

$$\frac{\partial X_5}{\partial L_{2,4}} = 1, \quad \frac{\partial X_5}{\partial L_5} = 4 - (M_6^2 + M_7^2), \quad \frac{\partial X_5}{\partial L_1} = (1 - M_7^2), \quad \frac{\partial X_5}{\partial L_3} = (1 - M_6^2). \qquad (33)$$

One new feature is the movement of A from its incompressible position towards the foremost point on the aerofoil, which, ignoring pressure waves, it should reach when $M_0 = 1$. The method of computing this movement has been given in the introduction. Since A is not on a mesh point interpolation formulæ are now needed when dealing with the infinity in L at A by the methods of R. & M. 2726[2]. These can easily be deduced from the equations given in this reference.

Relaxation in the supersonic patches is still possible, but somewhat less convergent than in the elliptical region of the differential equation. An essential requirement of relaxation is that the elimination of a residual at one mesh point should not involve the appearance of larger residuals at neighbouring mesh points (not including residuals already at these points). Examination of the relaxation pattern of Fig. 2 for $M > 1$, reveals that for this requirement to be fulfilled it may be necessary to eliminate a residual at one point by altering L at a neighbouring mesh point. This procedure works for a time but it has been discovered that when M reaches a certain value it becomes impossible to find a continuous solution for L, *i.e.*, it is not possible to eliminate all the residuals. It is however possible to arrange the unrelaxed residuals in pairs of opposite sign along the lines in the field, and to deduce from these the existence of a discontinuity in L lying between them. The magnitude and position of this shock-wave can also be deduced from the size of the residuals[7].

8. *Results for NACA* 16.—Table 2 sets out the pressure cofficients for each of the Mach numbers calculated.

In Figs. 4 and 5 are compared the experimental and theoretical results for $M_0 = 0{\cdot}4$ and $0{\cdot}65$. They compare well in the range $0 \leqslant x/c \leqslant 0{\cdot}6$, but, as can be expected, discrepancies appear near the trailing edge. However the theoretical results for $M_0 = 0{\cdot}75$ do not agree very well with the experimental results at any of $M_0 = 0{\cdot}75$, $0{\cdot}775$ and $0{\cdot}80$. It appears that the theoretical curve would correspond best to an experimental curve for a value of M_0 between $0{\cdot}775$ and $0{\cdot}80$. The main source of error is the boundary layer, and for these high Mach numbers the velocity peak moves rapidly towards the trailing edge where boundary layer effects cannot be ignored. Nevertheless the theoretical results for $M_0 = 0{\cdot}75$ reproduce the general features of the high-speed experimental curves, *e.g.*, the appearance of a velocity peak on the rear half of the aerofoil.

In Figs. 7, 8 and 9 show the theoretical equivelocity contours for $M_0 = 0{\cdot}40$, $0{\cdot}65$ and $0{\cdot}75$ respectively. Results for $M_0 = 0{\cdot}75$ were completed for the upper half of the plane only. Values in the lower half plane were changing quite slowly and to save time were estimated by extrapolation for this last case. The relaxation pattern for large values of M is such that residuals have little effect on mesh points in the ϕ direction, and so errors in the lower surface values would have little effect on the upper surface values. There is a suggestion of Prandtl-Meyer flow round the

nose in Fig. 9. The lines of constant velocity are almost the straight radial lines characteristic of this type of flow. A shock-wave appears to be impending towards the trailing edge.

Turning now to the results shown in Fig. 10 we notice that both the theoretical and experimental C_L against M_0 curves increase at a smaller rate than implied by the Glauert law

$$C_L = C_{L0}\sqrt{(1 - M_0^2)}. \quad .. \quad .. \quad .. \quad .. \quad .. \quad .. \quad .. \quad (34)$$

The displacement of the C_L curves by almost a constant percentage is due to the loss of lift near the trailing edge mentioned in section 6. Applying the Glauert law to the upper surface value of C_p actually underestimates it[6], but from both theory and experiment the lower surface value C_p decreases slightly instead of increasing. This explains why

$$C_L = \int (C_{p\,(\text{upper})} - C_{p\,(\text{lower})})\, d(x/c)$$

falls short of the value predicted by (34). The displacement of the curves in Fig. 11 is clearly due to the loss of lift near the trailing edge in the experimental results.

9. *Conclusions.*—The method appears to be satisfactory treatment of the compressible flow of an inviscid fluid about an aerofoil. Discrepancies with experiment appear at high Mach numbers due to the movement of the velocity peak towards the trailing edge, in the neighbourhood of which the boundary layer cannot be ignored. Better methods of dealing with the compressible flow have been developed, but an exact treatment of compressible flow throughout the field seems to demand a numerical approach of the type given in this paper.

If accurate experimental low-speed velocity distributions are available for an aerofoil an adaptation of the polygon method would enable the inviscid flow profile to be deduced, and subtracting the original profile from this would leave the boundary layer displacement thickness. Now if the compressible flow about the *deduced* profile were calculated, and the change in the boundary layer with increase of M_0 could be neglected, the results of the calculation should agree closely with experimental results.

The aerofoil chosen presented a difficult case for calculation as the nose was very sharp. The numerical work for an aerofoil with a larger nose radius would not be so lengthy.

Acknowledgments.—Thanks are due to Mrs. D. M. Wood, B.Sc., for her able assistance in the heavy computational work. This arrangement was made possible by a grant from the Aeronautical Research Council.

REFERENCES

No.	*Author*	*Title, etc.*
1	A. Thom	A Cambered Aerofoil Treated by Squares Methods. (Oxford University Engineering Laboratory Report No. 10. July, 1948). A.R.C. 11,652. (Unpublished.)
2	L. C. Woods	The Numerical Solution of Two-dimensional Fluid Motion in the Neighbourhood of Stagnation Points and Sharp Corners. (Oxford University Engineering Laboratory Report No. 27. October, 1949). R. & M. 2726.
3	L. C. Woods	Two-dimensional Aerofoil Design in Compressible Flow. R. & M. 2731. November, 1949.
4	A. Thom and Laura Klanfer	Compressible Flow past an Aerofoil. (Oxford University Engineering Laboratory Report No. 26. July, 1949). A.R.C. 12,476. (Unpublished.)
5	L. M. Milne-Thomson	*Theoretical Aerodynamics.* Macmillan and Co. 1948.
6	Liepmann and Puckett	*Aerodynamics of a Compressible Fluid.* Wiley and Sons. 1947.
7	L. C. Woods	A Relaxation Treatment of Shock Waves. A.R.C. 13,242. July, 1950. (Unpublished.)
8	L. C. Woods	Incompressible Two-dimensional Flow of an Inviscid Fluid about an Asymmetric Aerofoil. A.R.C. 13,395. (Unpublished.)

TABLE 1

Ordinates for 10 *per cent Aerofoil NACA* 16. 5 *in. Chord*

1 Dist. From L.E. in.	2 Upper Surface in.	3 Lower Surface in.	1 in.	2 in.	3 in.
0	0	0	2·0	0·3244	0·1636
0·005	0·0165	0·0146	2·1	0·3274	0·1649
0·010	0·0236	0·0202	2·2	0·3299	0·1659
0·015	0·0292	0·0243	2·3	0·3316	0·1666
0·02	0·0339	0·0277	2·4	0·3325	0·1671
0·025	0·0382	0·0306	2·5	0·3327	0·1673
0·03	0·0420	0·0332	2·6	0·3324	0·1671
0·035	0·0455	0·0356	2·7	0·3313	0·1666
0·04	0·0489	0·0377	2·8	0·3295	0·1658
0·05	0·0550	0·0416	2·9	0·3269	0·1645
0·06	0·0605	0·0450	3·0	0·3235	0·1628
0·07	0·0657	0·0481	3·1	0·3192	0·1607
0·08	0·0705	0·0509	3·2	0·3140	0·1580
0·09	0·0750	0·0535	3·3	0·3079	0·1548
0·10	0·0793	0·0559	3·4	0·3007	0·1511
0·125	0·0892	0·0613	3·5	0·2925	0·1467
0·15	0·0982	0·0660	3·6	0·2832	0·1417
0·175	0·1065	0·0702	3·7	0·2729	0·1361
0·2	0·1142	0·0741	3·8	0·2614	0·1299
0·25	0·1283	0·0809	3·9	0·2487	0·1231
0·3	0·1410	0·0868	4·0	0·2345	0·1156
0·35	0·1526	0·0921	4·1	0·2188	0·1076
0·4	0·1634	0·0968	4·2	0·2016	0·0989
0·45	0·1734	0·1012	4·3	0·1829	0·0897
0·5	0·1828	0·1053	4·4	0·1627	0·0797
0·6	0·2001	0·1125	4·5	0·1410	0·0690
0·7	0·2156	0·1189	4·6	0·1177	0·0576
0·8	0·2296	0·1245	4·7	0·0927	0·0455
0·9	0·2424	0·1297	4·8	0·0658	0·0327
1·0	0·2540	0·1345	4·9	0·0366	0·0192
1·1	0·2647	0·1389	5·0	0·005	0·005
1·2	0·2744	0·1429			
1·3	0·2833	0·1465		T.E. Radius 0·005	
1·4	0·2914	0·1498			
1·5	0·2987	0·1528			
1·6	0·3052	0·1555			
1·7	0·3100	0·1579			
1·8	0·3151	0·1601			
1·9	0·3206	0·1620			

TABLE 2

Pressure Coefficients

Upper Surface					Lower Surface			
x/c	$M = 0$	$M = 0{\cdot}4$	$M = 0{\cdot}65$	$M = 0{\cdot}75$	x/c	$M = 0$	$M = 0{\cdot}4$	$M = 0{\cdot}65$
−0·0008		(Stagnation Point)			0·0008		(Stagnation Point)	
0·0000	0·656	0·669	(Coarser Mesh		0·0044	0·888	0·921	
0·0001	0·345	0·340	used near		0·0068	0·814	0·840	
0·0005	0·084	0·063	nose).		0·0085	0·753	0·776	
0·0008	−0·103	−0·148	0·575	0·626	0·010	0·713	0·733	0·769
0·0017	−0·348	−0·407			0·012	0·625	0·641	
0·0027	−0·493	−0·550	0·005	0·134	0·014	0·594	0·609	0·620
0·0047	−0·698	−0·764	−0·383	−0·239	0·019	0·523	0·535	0·545
0·007	−0·788	−0·842	−0·569	−0·525	0·023	0·478	0·487	0·496
0·010	−0·836	−0·898	−0·894	−0·855	0·031	0·417	0·424	0·438
0·015	−0·828	−0·883	−1·004	−0·871	0·039	0·372	0·378	0·388
0·022	−0·738	−0·786	−0·938	−0·894	0·054	0·308	0·306	0·310
0·033	−0·706	−0·746	−0·902	−0·885	0·068	0·259	0·254	0·257
0·053	−0·658	−0·701	−0·858	−0·876	0·097	0·206	0·203	0·205
0·073	−0·625	−0·673	−0·819	−0·850	0·124	0·174	0·169	0·171
0·114	−0·570	−0·620	−0·758	−0·809	0·178	0·129	0·123	0·114
0·155	−0·535	−0·584	−0·726	−0·754	0·231	0·096	0·090	0·085
0·197	−0·506	−0·550	−0·681	−0·716	0·284	0·071	0·063	0·055
0·283	−0·482	−0·531	−0·660	−0·716	0·387	0·033	0·025	0·004
0·367	−0·474	−0·524	−0·655	−0·729	0·488	0·005	−0·005	−0·027
0·452	−0·467	−0·513	−0·644	−0·750	0·588	−0·019	−0·030	−0·058
0·543	−0·458	−0·507	−0·634	−0·790	0·686	−0·027	−0·040	−0·071
0·631	−0·443	−0·496	−0·619	−0·820	0·787	−0·001	−0·016	−0·031
0·715	−0·411	−0·460	−0·577	−0·701	0·836	0·025	0·014	0·006
0·802	−0·341	−0·386	−0·505	−0·537	0·887	0·070	0·059	0·055
0·848	−0·271	−0·305	−0·350	−0·370	0·915	0·103	0·095	0·090
0·895	−0·169	−0·193	−0·230	−0·239	0·940	0·150	0·139	0·140
0·918	−0·103	−0·119	−0·139	−0·145	0·968	0·225	0·212	0·215
0·942	−0·017	−0·026	−0·041	−0·045	1·000		(Stagnation Point)	
0·971	0·099	0·096	0·083	0·085				
1·000	(Stagnation Point)							

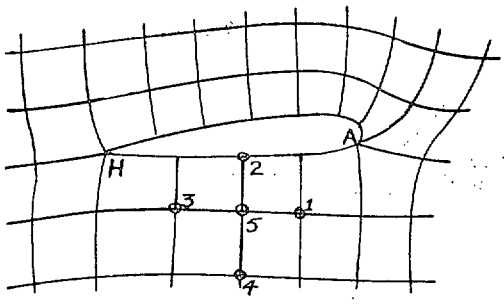

FIG. 1a. (x, y)-plane.

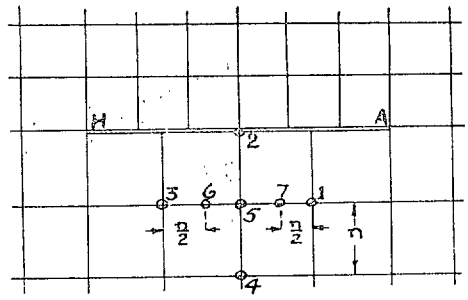

FIG. 1b. (ϕ, ψ)-plane.

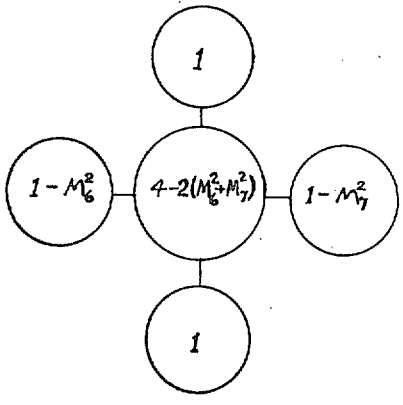

FIG. 2. Relaxation pattern.

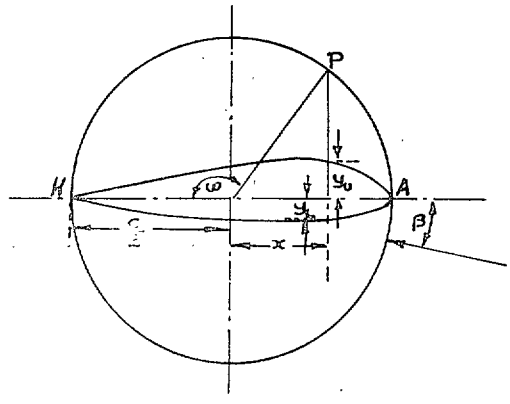

FIG. 3.

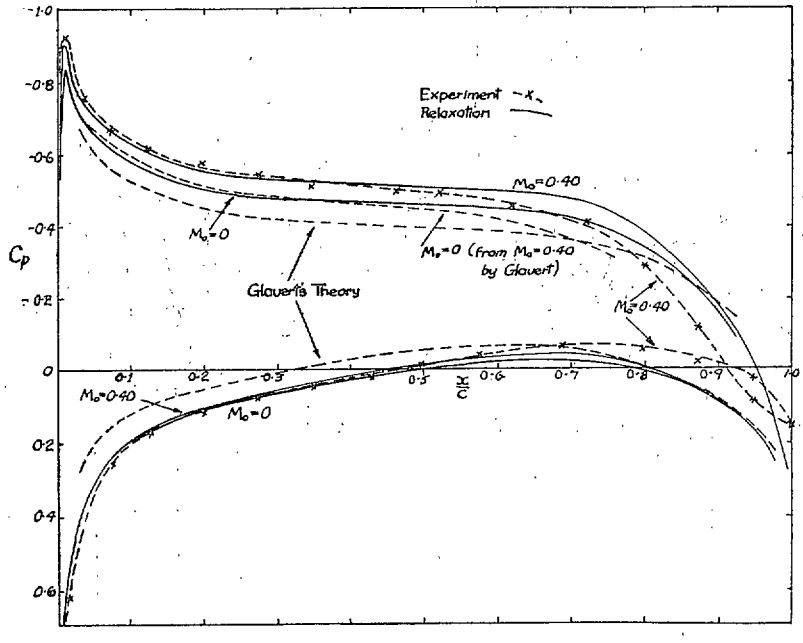

FIG. 4. Pressure distributions at $M_0 = 0, 0{\cdot}40$.

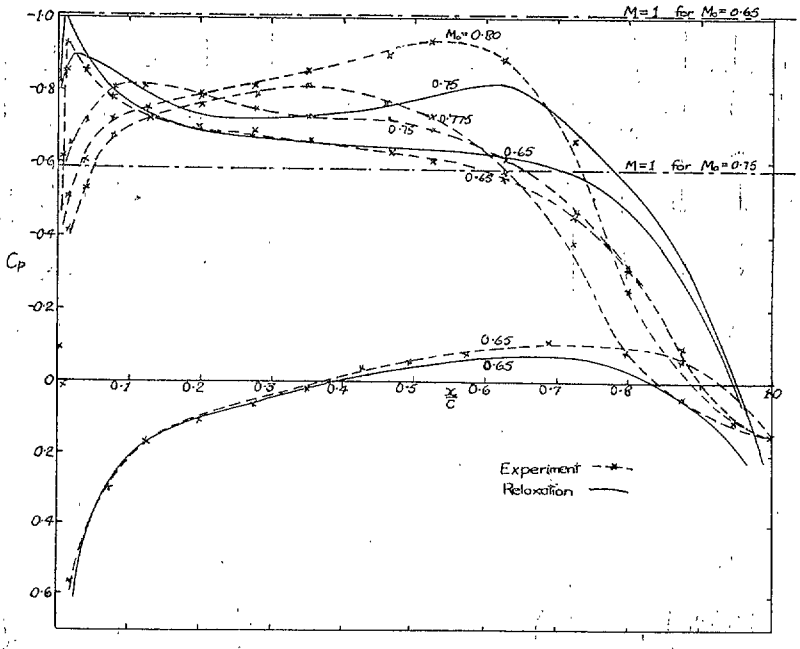

FIG. 5. Pressure distributions at $M_0 = 0{\cdot}65, 0{\cdot}75$.

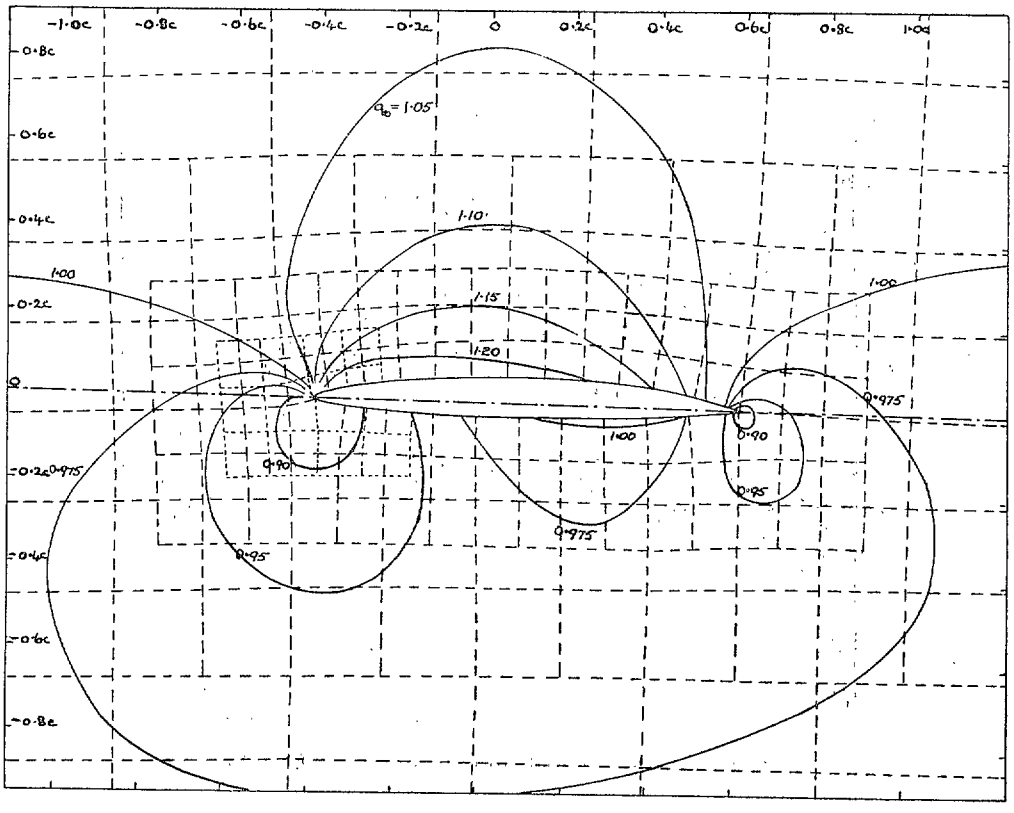

FIG. 6. Incompressible flow.

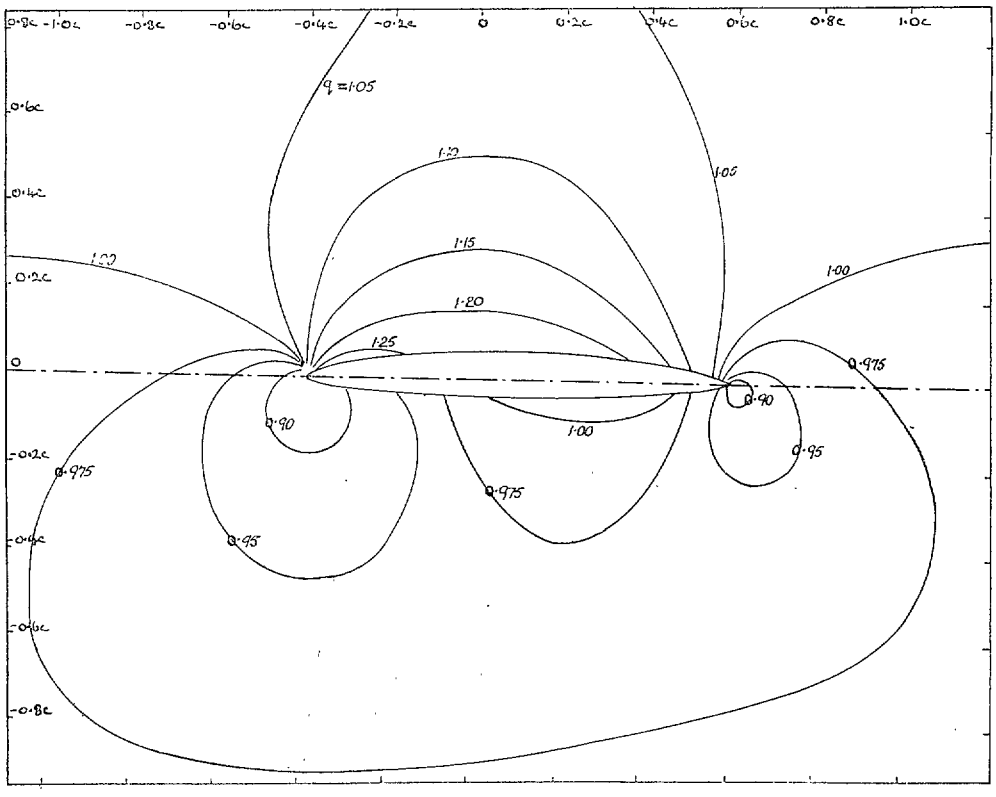

FIG. 7. Equivelocity contours at $M_0 = 0{\cdot}4$.

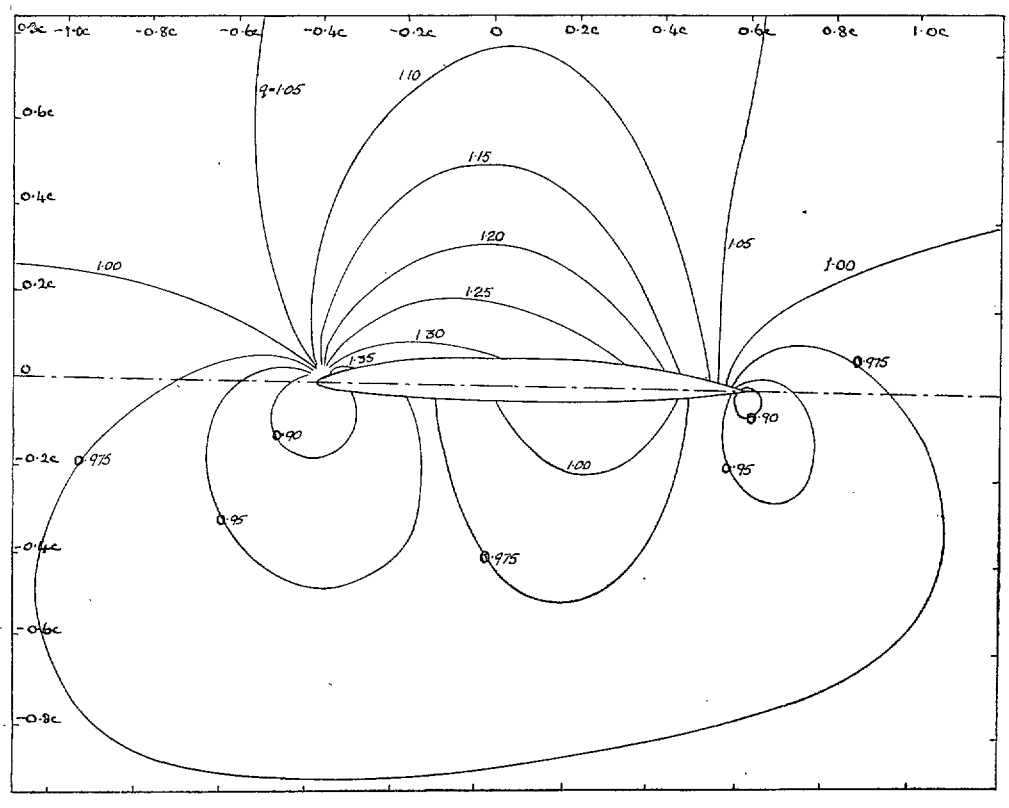

FIG. 8. Equivelocity contours at $M_0 = 0{\cdot}65$.

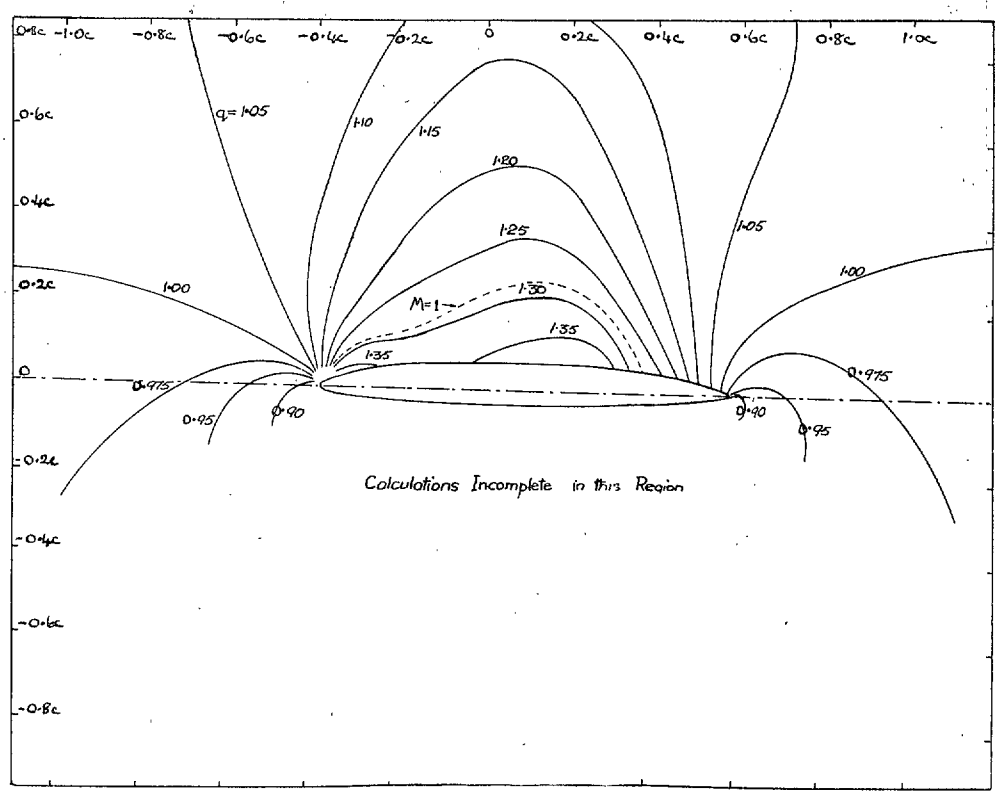

FIG. 9. Equivelocity contours at $M_0 = 0{\cdot}75$.

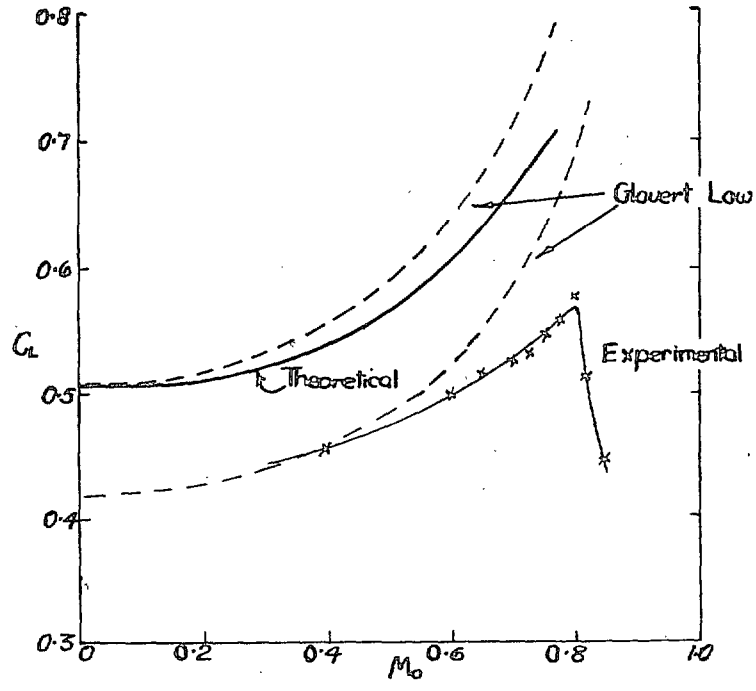

FIG. 10.

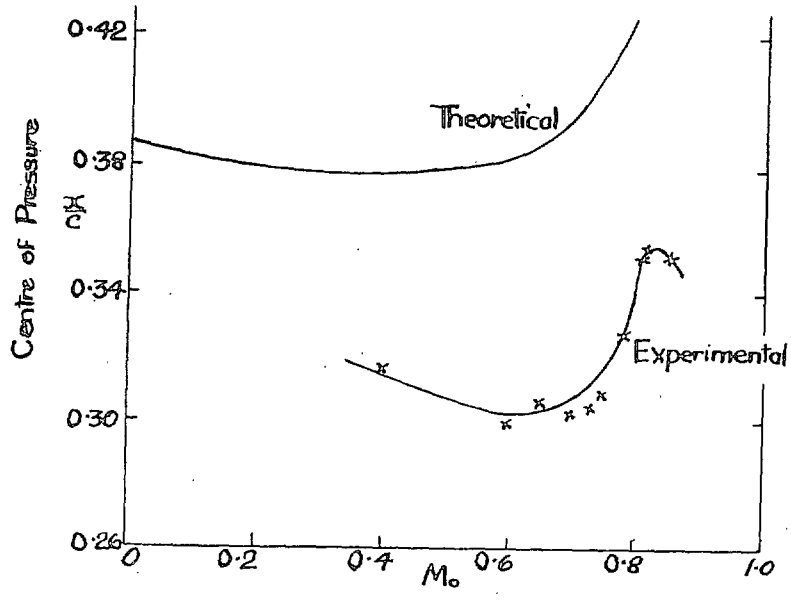

FIG. 11.

J4283 Wt.13/806 K9 10/53 D&Co. 34-263

PRINTED IN GREAT BRITAIN

Publications of the Aeronautical Research Council

ANNUAL TECHNICAL REPORTS OF THE AERONAUTICAL RESEARCH COUNCIL (BOUND VOLUMES)

1936 Vol. I. Aerodynamics General, Performance, Airscrews, Flutter and Spinning. 40*s.* (40*s.* 9*d.*)
Vol. II. Stability and Control, Structures, Seaplanes, Engines, etc. 50*s.* (50*s.* 10*d.*)
1937 Vol. I. Aerodynamics General, Performance, Airscrews, Flutter and Spinning. 40*s.* (40*s.* 10*d.*)
Vol. II. Stability and Control, Structures, Seaplanes, Engines, etc. 60*s.* (61*s.*)
1938 Vol. I. Aerodynamics General, Performance, Airscrews. 50*s.* (51*s.*)
Vol. II. Stability and Control, Flutter, Structures, Seaplanes, Wind Tunnels, Materials. 30*s.* (30*s.* 9*d.*)
1939 Vol. I. Aerodynamics General, Performance, Airscrews, Engines. 50*s.* (50*s.* 11*d.*)
Vol. II. Stability and Control, Flutter and Vibration, Instruments, Structures, Seaplanes, etc. 63*s.* (64*s.* 2*d.*)
1940 Aero and Hydrodynamics, Aerofoils, Airscrews, Engines, Flutter, Icing, Stability and Control, Structures, and a miscellaneous section. 50*s.* (51*s.*)
1941 Aero and Hydrodynamics, Aerofoils, Airscrews, Engines, Flutter, Stability and Control, Structures. 63*s.* (64*s.* 2*d.*)
1942 Vol. I. Aero and Hydrodynamics, Aerofoils, Airscrews, Engines. 75*s.* (76*s.* 3*d.*)
Vol. II. Noise, Parachutes, Stability and Control, Structures, Vibration, Wind Tunnels. 47*s.* 6*d.* (48*s.* 5*d.*)
1943 Vol. I. (*In the press.*)
Vol. II. (*In the press.*)

ANNUAL REPORTS OF THE AERONAUTICAL RESEARCH COUNCIL—

1933–34	1*s.* 6*d.* (1*s.* 8*d.*)	1937	2*s.* (2*s.* 2*d.*)
1934–35	1*s.* 6*d.* (1*s.* 8*d.*)	1938	1*s.* 6*d.* (1*s.* 8*d.*)
April 1, 1935 to Dec. 31, 1936.	4*s.* (4*s.* 4*d.*)	1939–48	3*s.* (3*s.* 2*d.*)

INDEX TO ALL REPORTS AND MEMORANDA PUBLISHED IN THE ANNUAL TECHNICAL REPORTS, AND SEPARATELY—

April, 1950 – – – – R. & M. No. 2600. 2*s.* 6*d.* (2*s.* 7½*d.*)

AUTHOR INDEX TO ALL REPORTS AND MEMORANDA OF THE AERONAUTICAL RESEARCH COUNCIL—

1909–1949 – – – – – R. & M. No. 2570. 15*s.* (15*s.* 3*d.*)

INDEXES TO THE TECHNICAL REPORTS OF THE AERONAUTICAL RESEARCH COUNCIL—

December 1, 1936 — June 30, 1939.	R. & M. No. 1850.	1*s.* 3*d.* (1*s.* 4½*d.*)
July 1, 1939 — June 30, 1945.	R. & M. No. 1950.	1*s.* (1*s.* 1½*d.*)
July 1, 1945 — June 30, 1946.	R. & M. No. 2050.	1*s.* (1*s.* 1½*d.*)
July 1, 1946 — December 31, 1946.	R. & M. No. 2150.	1*s.* 3*d.* (1*s.* 4½*d.*)
January 1, 1947 — June 30, 1947.	R. & M. No. 2250.	1*s.* 3*d.* (1*s.* 4½*d.*)
July, 1951 – – – –	R. & M. No. 2350.	1*s.* 9*d.* (1*s.* 10½*d.*)

Prices in brackets include postage.

Obtainable from

HER MAJESTY'S STATIONERY OFFICE

York House, Kingsway, London W.C.2; 423 Oxford Street, London W.1 (Post Orders: P.O. Box No. 569, London S.E.1); 13A Castle Street, Edinburgh 2; 39 King Street, Manchester 2; 2 Edmund Street, Birmingham 3; 1 St. Andrew's Crescent, Cardiff; Tower Lane, Bristol 1; 80 Chichester Street, Belfast OR THROUGH ANY BOOKSELLER